Interfacial properties of windmill palm fiber reinforced laminated veneer lumber (LVL) under high voltage electrostatic field (HVEF)

Zehui Ju, Tianyi Zhan, Nicolas Brosse, Yang Wei, Haiyang Zhang, Jianxin Cui, Xiaoning Lu

Interfacial properties of windmill palm fiber reinforced laminated veneer lumber (LVL) under high voltage electrostatic field (HVEF)

Zehui Ju[a,b], Tianyi Zhan[a*], Nicolas Brosse[b*], Yang Wei[c], Haiyang Zhang[a], Jianxin Cui[a], Liangsong Cheng[a,b], Xiaoning Lu[a*]

[a] College of Materials Science and Engineering, Nanjing Forestry University, Nanjing, 210037, PR China

[b] Université de Lorraine - INRAE - LERMAB - GP4W, F 54 000 Nancy - France

[c] College of Civil Engineering, Nanjing Forestry University, Nanjing, 210037, PR China

Abstract: The acid / alkali pretreatment of windmill palm fiber (WPF) and the application of high voltage electrostatic force (HVEF) technology were used to prepare WPF-reinforced laminated veneer lumber (LVL). The effects of acid / alkali pretreatment on the surface morphology, chemical composition, crystallinity and mechanical properties of WPF were investigated. Moreover, the effects of intensity of HVEF on chemical composition and wettability of WPF were analyzed. Based on the mechanical experiment of WPF reinforced LVL composites, the mechanism of acid / alkali pretreatment and HVEF for the reinforcement of the composite was systematically clarified. The results showed alkali treatment efficiently removed silica particles and cuticles on the fiber surface and produced windmill palm fiber

*Corresponding author: Tianyi Zhan, Xiaoning Lu, College of Materials science and engineering, Nanjing Forestry University, the People's Republic of China (PRC), 210037; Nicolas Brosse, Universite de Lorraine, F-54000 Nancy, 54000. Email address: tyzhan@njfu.edu.cn (T.Z.); Nicolas.Brosse@univ-lorraine.fr (N.B.); luxiaoning-nfu@126.com (X.L.).

(ALWPF) with relatively high Young's modulus and tensile strength (increased by 167.07% and 26.52%, respectively). After HVEF treatment, the increase of surface-active groups (- OH and - CHO) led to the increase of surface oxidation degree and water contact angle of WPF. Under the synergistic effect of acid / alkali pretreatment and HVEF, the interfacial properties between the adhesive and WPF were improved, which led to the effective improvement of the mechanical properties of WPF reinforced LVL. This study showed that the synergistic effect of acid / alkali pretreatment and HVEF not only broaden the application scope of WPF, but also provide insights into the engineering of LVL production.

Keywords: Windmill palm fiber, Acid / Alkali pretreatment, High voltage electrostatic field, Interfacial properties, Laminated veneer lumber composites

1.Introduction

In recent years, laminated veneer lumber (LVL) produced from fast-growing species for building materials has attracted increasing attention and research [1]. LVL not only has most of the properties of natural wood, but also has many excellent properties including high strength and toughness and good stability [2]. LVL has a wide range of applications, in the fields of non-structural bearing (including carriage board, furniture, floor, packaging materials) and structural bearing (including timber structure keel, room beam) [3]. However, the mechanical properties of LVL based on fast-growing wood are limited by recurring limitations such as low strength, poor toughness and dimensional stability [4]. Therefore, the production of LVLs from fast-growing woods has become a research hot spot in the wood

industry in order to expand their applicability in the field of load-bearing structures [5].

The reinforcement based on wood has become an important way to improve the comprehensive utilization rate of wood resources and the quality grade of wood products [6]. Currently, the most widely used composite materials are fiber-reinforced composites, which have excellent bending resistance and shear resistance, especially in the vicinity of the bending load [7]. Natural fiber is very attractive to structural materials, such as panel or wall materials, because natural fiber has low density, environment-friendly, low cost and easy availability, which can reduce construction time and environment pollution [8]. The natural fiber reinforcement materials include hemp, flax, bamboo fiber, coconut fiber, etc [9]. Flax fiber was widely used in car seats and door trims. Compared with the door trim made of traditional long fiber reinforced thermoplastic composites (LFT) and acrylonitrile butadiene styrene (ABS) plastics, the weight of the door trim made of natural fiber reinforced composites can be reduced by more than 20% [10]. The composites of flax and hemp with acrylated epoxidized soybean oil (AESO) can meet the strength requirements of housing applications, such as roof / wall panels and construction wood [11]. The ceiling made of hemp fiber and semi-rigid polyurethane elastomer has the advantages of simple process, higher strength and weight reduction of more than 10% [12]. The properties of composites depend on the properties of components and the interfacial compatibility between components [13]. Although natural fiber has good advantages, its main disadvantage is the poor interfacial performance between natural fiber and matrix, which leads to the insufficient interfacial force between the fiber and resin, the poor bonding interface performance, and greatly reduces the overall performance of fiber reinforced composites [14]. Therefore, it is urgent to explore new

fiber reinforced materials and efficient surface modification to improve the interfacial bonding properties between fiber and wood, so as to improve the mechanical properties of fiber reinforced wood composites.

Researchers have also been interested in wind palm fiber (WPF) in recent years [15]. The study on the mechanical properties of WPF shows showed that the breaking strength of WPF is higher, the fiber is longer, the linear density is much smaller than that of sisal fiber, the elongation at break is larger, and the initial modulus is close to that of pineapple leaf fiber [16]. In a single palm fiber, the fiber cells are closely arranged, the non-fiber cell content was relatively low [17]. WPF has good mechanical properties, and has been used as reinforcement in the fiber reinforced composites [18]. Surface morphology affects the adhesion between fiber and polymer, and surface modification can improve the application range of materials [19]. The mechanical properties of composites are largely determined by the adhesion between resin and fiber. In most cases, there is a regular arrangement of silica on the surface of the palm fibers. Tomlinson [20] proposed that silica in Palmae can be divided into two types: one is conical or cap shaped with parenchymatous basal cells, the other is rough or spiny spheroid with thick cell wall. A large number of hydrophobic substances are also present on the fiber surface, such as cerolipoid [21]. This complex surface composition of WPF improves their thermal and chemical stability but also reduces the adhesion between the fiber and the resin and limits their broad use. In the literature, it was found that the silica on the surface of jujube palm fibers could be peeled off by low concentration of alkali and acid solution, leaving annular holes [22]. Shanmugasundaram, N. et al. [23] showed that the impurities on the palm petiole fiber surface were gradually removed using an increasing

NaOH concentration of NaOH. For a concentration of 15%, the cell wall of the fiber surface was damaged and micro holes appeared, which increased the surface roughness and the adhesion between the fiber and the polymer. The above surface modification methods have a positive effect on the interfacial adhesion.

High voltage electric field (HVEF, > 1 kV) is used in the process of material preparation and modification as a treatment method which has a unique impact on the physical and chemical properties of materials [24]. Under the action of electric field, the excited free electrons collide with the chemical groups on the material surface, resulting in the formation of broken chemical bonds and new free electrons [25]. As a result, the polarization degree and surface free energy of the material surface are significantly improved. Kilic [26] measured the surface potential of the fiber material in the electric field. The results show that the surface energy of the fiber material increases and the resistivity decreases after the electric field treatment. The physical and chemical properties of biomass materials, adhesives and their bonding interface will be affected by HVEF. It is found that biomass materials can produce weak ionization by the action of electric field, which is caused by the movement of ions [27, 28]. In direct current (DC) electric field, the polarization phenomenon of biomass materials has the typical characteristics of ion ionization phenomenon [29]. Therefore, the application of HVEF in the hot-pressing process of the composite can increase the number of free electrons and chemical bonds between the material and the adhesive, which provides more chemical reaction sites to increase the conditions for the reaction between the material and the adhesive.

In this study, a combination of acid / alkali pretreatment and HVEF was used to improve

the surface properties of windmill palm fiber (WPF). The surface morphology, composition and properties of the treated WPF were examined in detail. The bond strength test of WPF-reinforced phenol-formaldehyde glue-based laminated veneer wood composites verified the enhancing effect of the treatment. The mechanical test of the composite was further carried out.

2. Materials and Experiments

2.1 Materials

The dimensions of 200 mm × 200 mm × 2.5 mm masson pine (*Pinus massoniana Lamb.*) veneers and phenol formaldehyde (PF) adhesive were provided from Lianyungang Nanfang Wood Industry Co., Ltd. (Jiangsu Province, P.R. China). In order to improve the bonding properties of wood veneer composites, the moisture content of masson pine veneers was adjusted at 7 ± 2% by oven-dried at 50 °C for 24 h, the average crack degree of masson pine veneer was 35%, and the density was 0.475g / cm^3. The PF adhesive of formaldehyde (F) / phenol (P) ratio was 2, the solid content of PF adhesive was 45 ± 2%, the viscosity was 132 mPa·s at room temperature, the density was 1.205 g / ml, and the pH was 13.5. Commercial WPF (*Trachycarpus fortunei*) fabric (1500 mm × 800 mm) was provided by Rugao Shuangma Chemical Co., Ltd. (Jiangsu Province, P.R. China). The consumption of woven WPF was 500 g/m^2, and it was woven using the "plain-weave" type of knitting. Sulfuric acid (98% solution), nitric acid (98% solution), sodium hydroxide, benzene and ethanol (95% solution) were produced by Nanjing Chemical Reagent Co., Ltd. (Jiangsu Province, P.R. China). The aluminum plates (300 mm × 300 mm × 1.5 mm) as electrode plates were provided from

Zhengguang metal material Co., Ltd. (Shandong Province, P.R. China.). A high voltage electrostatic generator (DISK-120K) was produced by Zhaomao coating Accessories Co., Ltd. (Guangdong Province, P. R. China).

2.2 Windmill palm fiber (WPF) pretreatment

In this experiment, alkali treatment and acid treatment were used to pretreat the windmill palm fibers. Two portions of windmill palm fibers with the same weight were put them in a 500ml beaker, and then added with 5 % sodium hydroxide solution and 5 % nitric acid solution respectively. The beakers were treated in a 70 ℃ water bath for 2 hours. After water bath treatment, the pretreated samples were taken out, cooled down, washed to neutral with distilled water, dried in oven at 70 ℃ for 12 hours. At last, the alkali treated windmill palm fiber (ALWPF) and acid treated windmill palm fiber (ACWPF) were prepared.

2.3 Preparation of windmill palm fiber reinforced laminated veneer lumber composites

The WPF reinforced plywood composites were prepared under different treatments of WPF and different high voltage electrostatic field (HVEF) strength to study the effect of treatment methods on the interfacial properties of plywood. The three-layer WPF reinforced composites were assembled by double-sided gluing process, and the gluing amount of PF adhesive was 150g / m^2. The composites were put into a hot press with high-voltage electrostatic device for hot pressing. The high voltage electrostatic device contained two aluminum electrode plates, one of which was connected to the high voltage electrostatic generator, the other was connected to the ground, and the composites were placed between the two plates. The

hot-pressing parameters of plywood were as follows: the temperature was 140 °C, the pressure was 1.2 MPa, the hot-pressing time was 1.5min/mm, HVEF treatment time was the same as hot pressing time, and the electrostatic generator was stopped immediately after reaching the treatment time. The plywood assembly method and hot-pressing process with HVEF were shown in **Fig. 1**. The reinforced materials contained raw windmill palm fiber (RWPF), ALWPF and ACWPF. The parameters of HVEF included 0 kv, 20 kV, 40 kV, 60 kV. Each experiment was repeated 10 times.

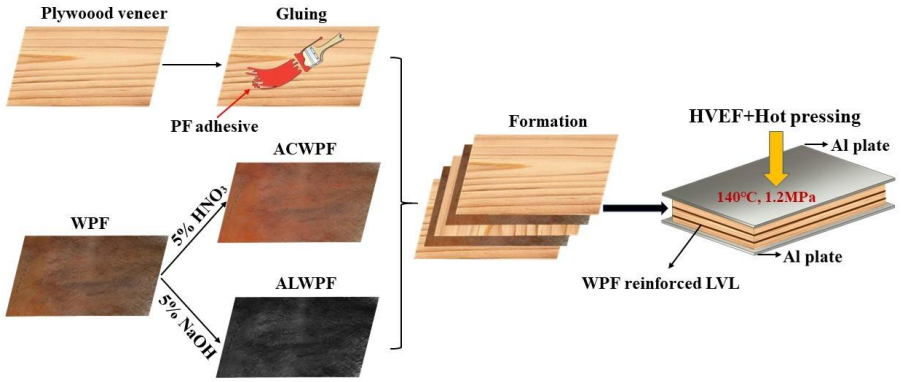

Figure 1 Schematic diagram of preparation of WPF reinforced LVL

2.4 Characterization methods

The structure of the material was analyzed by Fourier transform infrared spectroscopy (FTIR, TENSOR-27, Bruker, Germany) in this experiment. The samples were ground into powder and screened with 100 screens. Then, the powder was mixed with potassium bromide (KBr) and pressed tablets. The wavenumber scanning range was 4000 - 400cm^{-1}, and the resolution was 1cm^{-1}. Environmental scanning electron microscopy (ESEM, JSM-7800F, JEOL, Japan) was used to observe the surface morphology of the samples. The samples were fixed on the stage with conductive adhesive and plated with gold. Then, the samples were

placed in the ESEM, and the accelerating voltage was set at 10-15kV. The ESEM was equipped with X-ray energy dispersive spectrometer (EDS, Inca X-Max, Oxford, UK), which can be used for analysis chemical composition of samples. The acceleration voltage of EDS was 20kV. X-ray photoelectron spectroscopy (XPS, AXIS-HSi, Kratos, Japan) was used to analyze the chemical states of the elements in the samples. The pure magnesium Kα was used as the X-ray source. The vacuum degree of XPS was lower than 1.33×10^{-10} Pa. The X-ray power was 150W, the narrow sweep energy was 20 eV, the step size was 0.1eV, and the number of scans was 3 times. The internal standard method was used to eliminate the charging effect. The binding energy C1s (284.8ev) of the hydrocarbon was used for energy correction. The samples were analyzed by X-ray powder diffraction (XRD, XD-3, Beijing, China). The experimental conditions were: the pure copper Kα radiation (k) was 1.5418 Å, the acceleration voltage was 36 kV, the current was 20 mA, the scanning step size was 0.02 °, scanning ranged from 5 ° to 90 °, the scanning speed was 2 ° / min. The crystallinity of the samples can be determined quickly by the empirical crystallinity index [30].

2.5 Chemical composition analysis of windmill palm fiber

The cellulose, hemicellulose and lignin of raw materials were determined by NREL method [31]. The dried sample (300mg) which had been extracted by benzene alcohol mixture (benzene / ethanol (95%) ratio of 2 / 1, Soxhlet extraction) for 6h was put into a 100mL bottle. Three groups of parallel samples were prepared. 72% concentration of sulfuric acid (3mL) was evenly added to the bottle. Then the bottle was put in a 30 ℃ water bath for 1h, and kept shaking during the reaction. The bottle was take out, and added 84mL distilled water. The

193 tightly capped bottle was putted into the autoclave at 121 ℃ for 1 h. After the acid hydrolysis,
194 the mixture was separated by filtration. The absorption value of the diluted liquid was
195 determined by UV spectrophotometer at 205nm, and the absorption value was kept between
196 0.7 and 1.0. At the same time, the pH of the filtrate was adjusted to 1-3, and the contents of
197 glucose, xylose, arabinose and other monosaccharides were determined by HPLC. The solid
198 was washed with distilled water and dried for 24 h at 105 ℃. The calculation formulas were
199 as follows:
200 Calculation formula of acid-soluble lignin (ASL) content

201 $$ASL = \frac{Dilution\quad factor \times Absorption\quad value \times Filtrate\quad volume}{Absorption\quad coefficient(110) \times Dried\quad sample} \times 100\% \qquad (1)$$

202 Calculation formula of acid-insoluble lignin (AIL) content

203 $$AIL = \frac{Dried\quad residual}{Dried\quad sample} \times 100\% \qquad (2)$$

204 Calculation formula of cellulose content

205 $$Cellulose = \frac{Glu\cos e\quad concentration \times 0.9 \times Filtrate\quad volume}{Dried\quad sample} \times 100\% \qquad (3)$$

206 Calculation formula of hemicellulose content

207 $$Hemicellulose = \frac{Xylose\quad arabinose\quad concentrations \times 0.88 \times Filtate\quad volume}{Dried\quad sample} \times 100\% \qquad (4)$$

208

209 2.6 Fineness measurement of windmill palm fiber

210 Fiber fineness referred to the degree of fiber thickness, which was usually measured by
211 linear density and physical thickness. The larger the linear density was, the thicker the fiber
212 was. The fineness of fiber was measured by the cut-middles method. Firstly, the fiber was
213 straightened, the free fiber and the fiber shorter than the test length (*Lc*=10 mm) were

removed, then the fiber was cut. Each experiment was repeated 5 times. The calculation formula of fiber linear density was as follows:

$$T_t = 10^3 G/nLc \quad (5)$$

Where G was the weight of middle fiber, n was the number of fiber, and T_t was the linear density of fiber.

2.7 The mechanics property analysis of WPF

The mechanics property of WPF was measured by ASTM C1557-14 [32]. The stretch length was set to 30 mm in this experiment. The electronic universal strength testing machine (WDW3050, Jilin, China) was used to test the tensile strength of windmill palm fiber samples. The tensile speed was 0.5 mm / min, and each experiment was repeated 15 times. The fiber diameter was measured by optical microscope. Ten test points were taken for each fiber, and the average value was taken as the fiber diameter. The cross-sectional area of the fiber was calculated by using the formula of circle.

2.8 Electron spin resonance measurement

The electron spin resonance (ESR, EMX 10 / 12, Bruker, Germany) were used to measure the content of free radicals in the samples. The sample size was 40mm × 350 ± 20μm (length × diameter). The sample was oven-dried at 103 °C for 48h (the moisture content was less than 4%). Each experiment was repeated for 10 times.

2.9 Wettability property of WPF

The wettability properties of WPFs were characterized by the contact angle test (the sessile drop method). The moisture content of WPF was controlled at 4%. The WPF was fixed on the automatic video micro contact angle measuring instrument (DCAT 21, DataPhysics, Germany). 3 μL distilled water was deposited on the fiber surface. The clear images can be obtained by the optical imaging system. The contact angle was calculated by SAC20 software. Each sample measured 10 points, and the average was the contact angle of the WPF.

2.10 Mechanical properties and digital image correlation

The mechanical properties of WPF reinforced plywood were tested by electronic universal strength testing machine (CMT 4304, Shenzhen, China). The modulus of elasticity (MOE) of WPF reinforced plywood was measured according to EN-310-1993 [33]. The sample size was 300 mm × 50 mm (length × width). The bonding strength (BS) was tested according to EN-314-1-2004. The determination of dipping peeling performance was analyzed according to the China National Standard (GB / T 19536-2015 [34]) for class I plywood. The sample size was 100 mm × 25 mm (length × width), and the loading speed of universal strength testing machine was 1 mm / min. Each condition was repeated 10 times. Digital image correlation was used to record the strain of the sample during the bonding strength test. The image correlation was performed using the commercial software package Correlated Solutions (www.correlatedsolutions.com). After the calibration of the reference ruler, two CCD cameras were used to record the experimental process according to a photo every 0.1 second, and the resolution was 30 μm.

3. Results and Discussion

3.1 Characterization of acid / alkali pre-treated windmill palm fiber

3.1.1 Morphology of pre-treated windmill palm fiber

The surface of WPF (**Fig. 2a**) is unsmooth and has a fish scale morphology. Previous studies have shown that these "fish scale" substances were mainly composed of silica [19] which was supported by the results of microanalysis (EDS analysis) shown in **Fig. 2b**. After acid treatment, the silica component of the ACWPF surface (**Fig. 2c**) was partially removed, and the longitudinal gullies were exposed on part of the fiber. The silica fell off from the holes, and most of it was also scattered on the surface of the palm fiber. As shown in **Fig. 2d**, the longitudinal gullies of palm fibers were deepened after alkali treatment, which suggested that palm fibers were bundles, composed of several single fibers. Most of silica fell with the lignin, pectin and other substances, and a small amount of residual silica was dispersed on the fiber surface, which caused the fibers to be exposed, thus promoting the surface performance of palm fiber, exposing the active hydroxyl groups, and improving the wetting performance of the fiber [18]. The surface of the treated fibers revealed micro holes, as shown in **Fig. 2c** and **2d**.

Figure 2 Morphology of different windmill palm fiber. (a) RWPF. (b) microanalysis spectra (EDS analysis) of RWPF. (c) ACWPF. (d) ALWPF.

Figure 2 Morphology of different windmill palm fiber. (a) RWPF. (b) microanalysis spectra (EDS analysis) of RWPF. (c) ACWPF. (d) ALWPF.

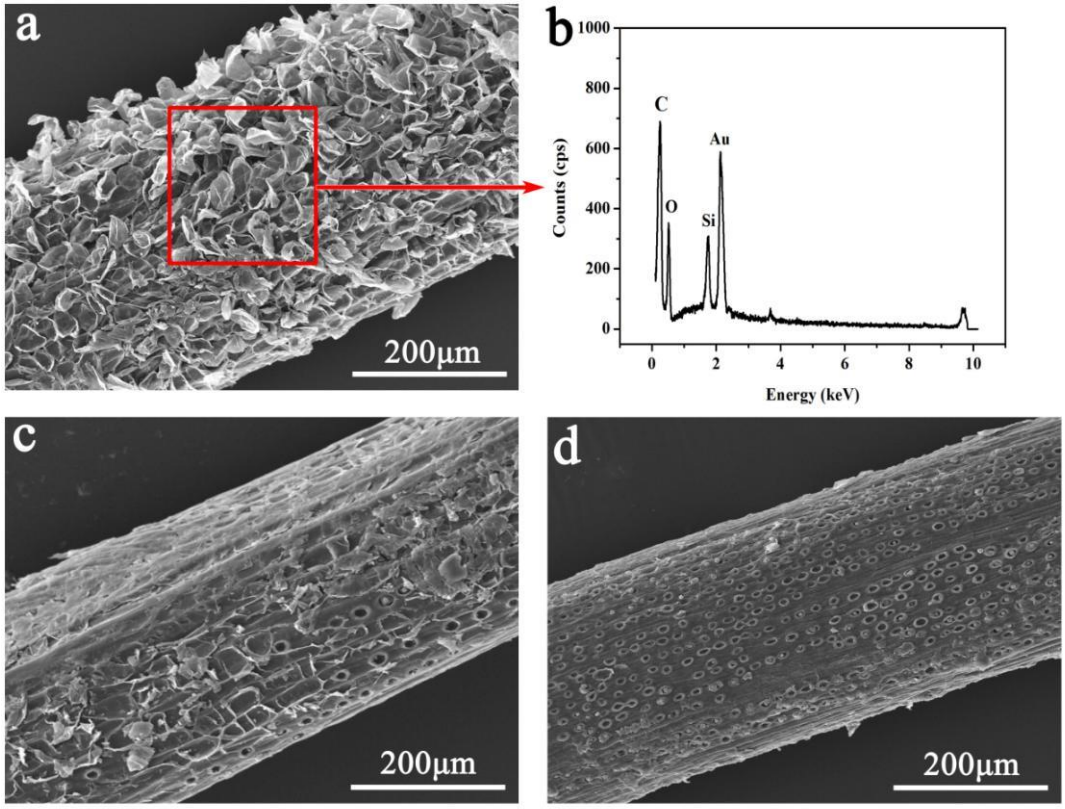

Figure 2 Morphology of different windmill palm fiber. (a) RWPF. (b) microanalysis spectra (EDS analysis) of RWPF. (c) ACWPF. (d) ALWPF.

At the same time, the hydrophilicity of the fiber was improved by the removal of hydrophobic substances such as silica [19]. The change of surface properties also meant that the surface properties of the fiber were improved when it was used in composites. The silica removal was confirmed by Elemental Analysis (**Table 1**). The Si% decreased from 3.86% for RWPF to 0.97% and 0.07% for ACPF and ALPW respectively.

Table 1 Elemental analysis of windmill palm fiber

Elemental	C (%)	O (%)	Si (%)
RWPF	46.45	49.68	3.86
ACWPF	50.69	48.34	0.97

ALWPF	55.74	44.19	0.07

3.1.2 Chemical composition and structure of windmill palm fiber

It can be seen from **Table 2** that the WPF chemical composition was strongly changed after acid / alkali treatment. After alkali treatment, the content of cellulose increased from 28.16% to 51.80%, lignin and hemicellulose decreased from 44.07% to 35.46% and from 20.60% to 9.90% respectively. The content of cellulose also increased after acid treatment, and lignin decreased significantly from 44.07% to 35.46%. This indicates that lignin and hemicellulose have chemical changes by acid / alkali treatment, and the original polymer macromolecules were hydrolyzed.

Table 2 Major chemical compositions of the windmill palm fiber

Composition	Cellulose	Lignin	Hemicellulose
RWPF	28.16	44.07	20.60
ACWPF	42.30	36.98	14.35
ALWPF	51.80	35.46	9.90

In order to further analyze the effect of acid / alkali treatment on the chemical composition of palm fiber, FTIR analysis was carried out. **Fig. 3** showed the FTIR spectra of WPF after different treatment. According to **Table S1**, the main functional groups on the material surface before and after pretreatment can be compared [19]. 3412 cm^{-1} is the O-H stretching vibration peak. The peak at 1737cm^{-1} is the characteristic absorption peak of carboxyl group in ferulic acid and p-Coumaric acid, which is the characteristic peak of hemicellulose. The absorption

peaks at 1602 cm^{-1} and 1507 cm^{-1} are the skeleton vibration peaks of aromatic ring, which are the characteristic peaks of lignin.

- After acid / alkali treatment, the peak at 2916 cm^{-1} which represents the symmetric stretching vibration of -CH_2 was obviously slowed down. They are the characteristic absorption peak of cellulose, and also the characteristic absorption peak of hydrophobic fatty acids and cerolipoid. The flat absorption peak indicated that hydrophobic substances were removed [35].

- The characteristic peaks of ACWPF at 1737 cm^{-1}, 1602 cm^{-1} and 1507 cm^{-1} became slower, indicating that hemicellulose and lignin were removed partly;

- There was no characteristic absorption peak in 1737 cm^{-1} of ALWPF, which meant that alkali treatment could remove hemicellulose in WPF, and it was an effective method to remove hemicellulose. The absorption peak at 1602 cm^{-1} became flat, indicating that lignin was removed slightly [17].

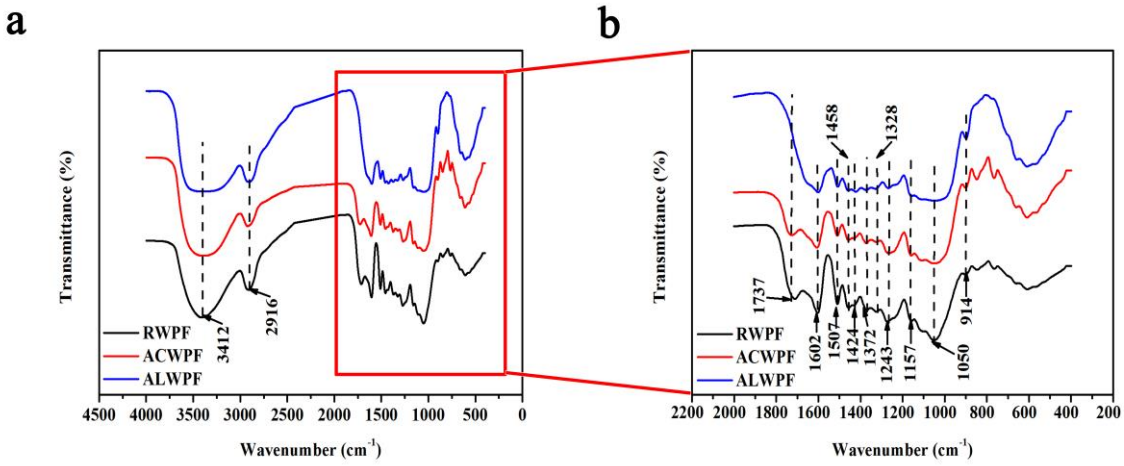

Figure 3 FTIR spectra of windmill palm fiber with different treatments for the wave numbers of (a) 4000 to 400 cm^{-1}, and (b) 2000 to 400 cm^{-1}.

In addition, 1157 cm^{-1} and 1050 cm^{-1} are the stretching vibration of ether bond (C-O) in the

glucose of cellulose, and the peak at 914 cm^{-1} is weak, which is attributed to the β- Glycosidic bond of cellulose monosaccharides. These characteristic peaks belong to cellulose absorption peaks. The shape and strength of palm fiber were enhanced after acid / alkali treatment, which proved that the content of cellulose in palm fiber increased [35].

3.1.3 Aggregated structure of windmill palm fiber

The X-ray diffraction pattern of WPF, ALWPF and ACWPF are given in **Fig. 4a** The main diffraction peaks of palm fiber were 16.2 ° (101), 22.1 ° (002) and 34.5 ° (040)，corresponding to cellulose I. Segal et al. [30] proposed that crystallization index can be used to characterize the crystallinity of natural cellulose. The higher the crystallization degree, the higher the crystallinity of natural cellulose. **Fig. 4b** was the crystallization index of raw and pretreated palm fiber. The crystallinity index was relatively low for the raw fibers (RWPF 34.2%) but increased after acid or basic treatment to reach 37.3% and 46.4% respectively due to hemicellulose, lignin and cerolipoid removal.

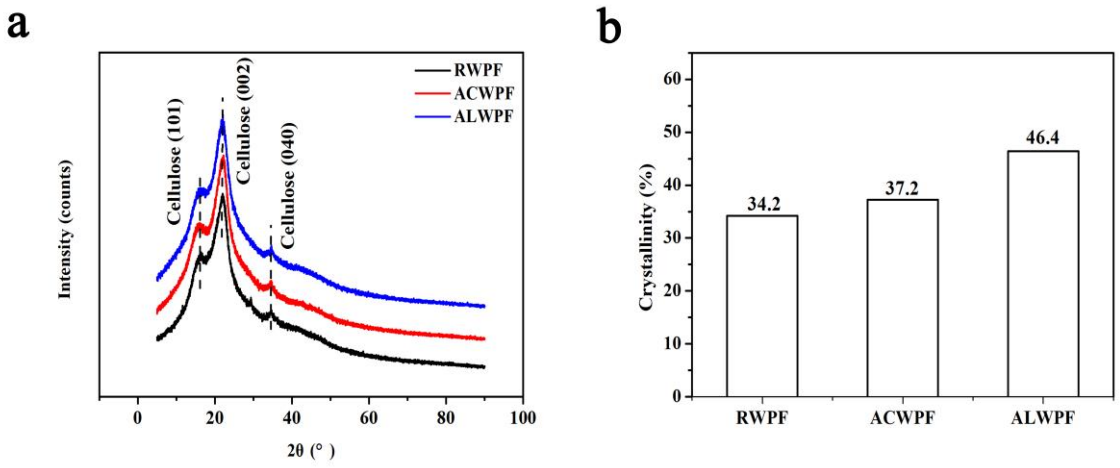

Figure 4 (a) X-ray diffraction patterns of different treatments; (b) Fiber crystallinity of different treatments

338 *3.1.4 Mechanical characterization of windmill palm fiber*

339 Fiber fineness was usually measured by linear density and geometric size. The larger the
340 linear density, the thicker the fiber, the larger the diameter. The diameter of fiber had an effect
341 on the tensile properties, the larger the fiber diameter, the lower the tensile strength. The linear
342 density of RWPF was 39.74 tex, which was in accordance with a previous study dealing with
343 palm fibers [36] and larger than other natural fibers (such as jute, sisal, flax, etc.) [16]. The
344 results in **Table 3** show that the linear density of treated fibers decreased, probably because of
345 the removal of components on the fiber surface, as shown in **Fig. 2c** and **2d**. The cross section
346 of WPF was composed of vessel, sieve tube, sclerenchyma and phloem tissue, so there is a
347 certain cavity in the palm fiber. The previous study showed that the cell wall was swelled to a
348 certain extent in the alkali treatment, which made the cell wall thicker, the cavity smaller and
349 the hollowness decreased [37]. Therefore, when the fiber diameter is reduced, the cavity size
350 is lower, and the cell wall becomes thicker, the material can bear more tensile force and show
351 better mechanical properties at the same conditions.

352 **Table 3** Fineness and mechanical properties of windmill palm fiber by different pretreatments

	RWPF	ACWPF	ALWPF
Linear density (tex)	39.74 ± 4.67	32.55 ± 2.01	24.37 ± 1.82
Modulus (Gpa)	2.46 ± 0.85	3.45 ± 0.34	6.57 ± 0.46
Breaking strength (Mpa)	309.94 ± 12.94	324.96 ± 7.29	392.13 ± 4.52
Elongation at break (%)	26.58 ± 4.32	24.15 ± 3.13	23.60 ± 3.41

353

354

355 The mechanical properties of treated palm fiber were shown in **Table 3**. It can be seen that

the tensile strength of treated palm fibers increased slightly. These results agree with previous works done on jute and palm fibers [38,39]. When hemicellulose was removed, the fibers may be became not compact and the rigidity became smaller, so that the fibers can rearrange themselves along the tensile deformation direction. The softening of the fibers affects the stress transfer between the raw fibers, thus affecting the increase of fiber stress under tensile deformation. With the removal of lignin, the micropores of the fibers are gradually eliminated, resulting in the middle sheet connecting the cells was more plasticity and uniformity. Hemicellulose is a kind of disordered and irregular nonlinear material, so its mechanical properties are poor. The removal of partial hemicellulose is beneficial to increase the mechanical properties of the fiber. The significant increase in modulus and tensile strength observed for alkali-treated fibers (6.57 GPa and 392.13 MPa, respectively), can be explained by the greater removal of non-cellulosic polymers associated to the increase of crystallinity previously described (**Fig. 4b**). It has been also described that alkali treatment of natural fibers can reduce the spiral angle of cellulose microfibers. However, Beckermann et al. [40] reported that alkali treatment reduced the strength of untreated fibers, which may be due to the degradation of cellulose chain after alkali treatment. From **Fig. 2c**, some materials (lignin, wax and oil) were removed from the fiber surface after acid treatment, which may be the reasons for the increase of tensile strength and Young's modulus of ACWPF. Different from alkali treatment, the modulus and breaking strength of ACWPF were slightly higher than that of RWPF. It showed that acid treatment method has little effect on the mechanical properties of the composites.

After hemicellulose and lignin were removed, the elongation at break decreased, and the

values were shown in **Table 3**. The elongation at break of RWPF was 26.58% when the stretch length was 3 cm. After acid treatment and alkali treatment, the elongation at breaks of ACWPF and ALWPF had almost results with 24.15% and 23.60%, respectively. The higher elongation at break makes the palm fiber used as an elastic reinforcing material for the preparation of composite materials [38].

3.2 Effect of HVEF on windmill palm fiber and PF adhesive

3.2.1 FTIR analysis

The surface functional groups of WPF and PF adhesive after HVEF were first analyzed by FTIR (suppl materials **Fig. S1**). After HVEF treatment, the oxygen-containing functional groups of WPF increased to a certain extent [41]. However, this change was not significant. Due to the limitation of this technology in effective depth penetration, especially in the short wavenumber region, the change of functional groups caused by HVEF cannot be evidenced by FTIR [1]. Therefore, XPS analysis was used to better comprehending the chemical mechanism of WPF treated by HVEF.

The characteristic peaks of main chemical groups in PF adhesive were summarized in **Table S2** [41]. It can be seen from **Fig. S1d** that the characteristic peaks at 3412 cm^{-1} (O–H stretching vibration), 2916 cm^{-1} (C–H stretching vibration), 1602 cm^{-1} (C=C stretching vibration), 1450 cm^{-1} (CH_2 shear vibration), 1213 cm^{-1} (C–O stretching vibration, O–H bending vibration) and 1017 cm^{-1} (C–O stretching vibration) increased significantly by HVEF treatment. With the increase of voltage, the intensity of these characteristic peaks increased significantly, and the change rate changed with different voltage. At the condition of 60kV, the

intensity of each characteristic peak was the highest compared with that of untreated PF adhesive. These results were mainly attributed to the strong ionization of a large number of water and oxygen molecules in the air under HVEF, and the formation of new electrons, hydrogen ions, oxygen ions, hydroxyl and other chemical groups increased significantly [42]. These chemical groups impact the glue, which improved the polarity and charge density of the adhesive. With the increase of voltage, the excited chemical groups increased, which was beneficial to increase the content of hydroxymethyl. At a certain temperature, hydroxymethyl was participated in the polycondensation of the adhesive. The increase of methylene bond in the treated adhesive improved the chemical reactivity of the adhesive. At the same time, a large number of excited electrons and broken chemical bonds (oxygen-containing groups) were collided with the adhesive and reacted with each other, increasing the cross-linking reaction of the resin.

3.2.2 XPS analysis

The changes of chemical elements such as oxygen and carbon on the material surface were qualitatively analyzed by X-ray photoelectron spectroscopy. **Table S3** shows the main distribution of C1s in WPF components [43]. **Fig. 5** is the deconvolution of high resolution C1s XPS spectra. **Table S4** summarizes the XPS element analysis of WPF for the different pretreatments (C1s%, O1s%), O / C ratio and deconvolution data of the C1s signals. The carbon content and oxygen content of RWPF surface were 76.29% and 23.71%, respectively. After acid / alkali treatment, the carbon content decreased to a certain extent and the oxygen content increased relatively, which confirmed the partial removal of hemicellulose and lignin

after acid / alkali treatment previous observed (section 3.1) [36]. After HVEF treatment (60 kV), the O / C ratio of RWPF, ACWPF and ALWPF increased significantly by 35.48%, 36.11% and 47.06%, respectively. The results showed that the oxygen-containing chemical groups on the materials surface were increased by HVEF treatment. According to literature data, this observation is attributed to the fact that HVEFs generate active entities in the air which can oxidize the surface of the material [44]. The reason for the greater increase for ALWPF is that the fiber surface is more accessible and exposed after alkaline treatment.

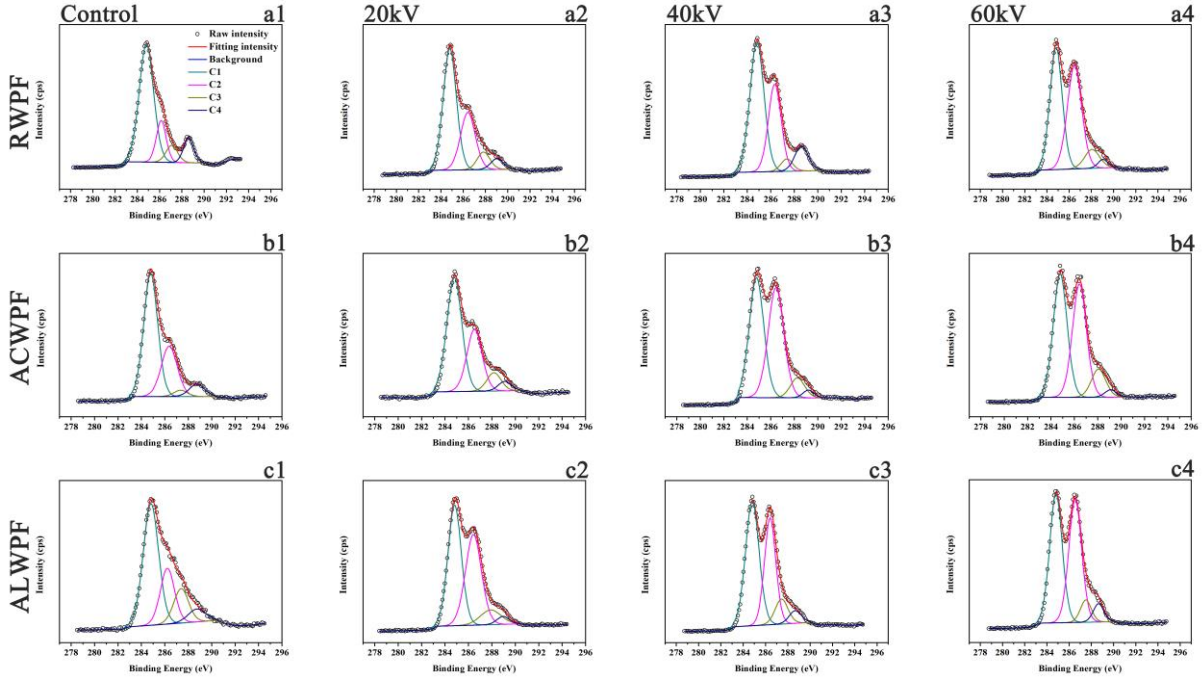

Figure 5 High resolution of XPS spectra with C1s divided into C1, C2, C3 and C4 components for different treatments

The results from **Fig. 5** and **Table S4** showed that the C1, C2, C3 and C4 peaks of RWPF, ACWPF and ALWPF changed significantly after HVEF treatment. The C2, C3 and C4 components of RWPF-60 increased by 31.92%, 28.68% and 15.15%, the C2, C3 and C4 components of ACWPF-60 increased by 34.86%, 61.61% and 17.32%, the C2, C3 and C4

components of ALWPF-60 increased by 39.74%, 71.15% and 15.35%, and C1 component decreased significantly. This may be explained by the fact that a large number of broken oxygen-containing chemical groups by HVEF treatment reacted with the groups (– OH and – CHO) on the material surface, which significantly improved the degree of polarization and oxidation of the material surface [45]. The change of C1s composition indicated that the increase of oxygen-containing functional groups on the WPF enhanced the surface wettability. With the increase of treatment voltage, C2, C3 and C4 components increase significantly, while C1 component decreases. This trend is in accordance with an increase of oxygen-containing groups content and a higher WPF surface reactivity [44, 46]. However, with a further increase of the voltage, the each component change rate decreased, which was mainly due to the existence of limit value in the process of HVEF induced effect [47].

3.2.3 Contact angle and surface free energy

Fig. 6 shows the results of water contact angle and surface free energy on the different WPF treated by HVEF. As shown in **Fig. 6a**, the contact angle (IA) decreased markedly after HVEF treatment and with an increase of treatment intensity. Compared with the untreated different WPF, the IA of RWPF-60, ACWPF-60 and ALWPF-60 decreased from 109.09 ° to 85.32 °, from 92.83 ° to 65.41 ° and form 66.96 ° to 50.22 ° respectively.

The effect of different HVEF treatment voltage on the surface free energy of different WPF was shown in **Fig. 6b**. The total free energy (T), dispersed component (DC) and polar component (PC) on the surface of WPF effectively increased by HVEF treatment, and the surface free energy of ALWPF changed the most after HVEF treatment. Compared with

ALWPF-0, DC of ALWPF-60 increased from 37.2 mJ / m^2 to 53.4 mJ / m^2, and PC of ALWPF-60 increased from 16.7 mJ / m^2 to 23.6 mJ / m^2. Due to the high polarity of the oxygen-containing functional groups, the surface polarity of palm fiber was improved. With the increase of voltage, the change rate of each component decreased, which was mainly due to the existence of limit value in the process of HVEF induced effect [47]. Based on the above analysis, we proved that HVEF treatment was beneficial to the excitation of oxygen-containing functional groups on the WPF surface in a short time. The results showed that HVEF treatment enhanced the hydrophilicity of WPF surface.

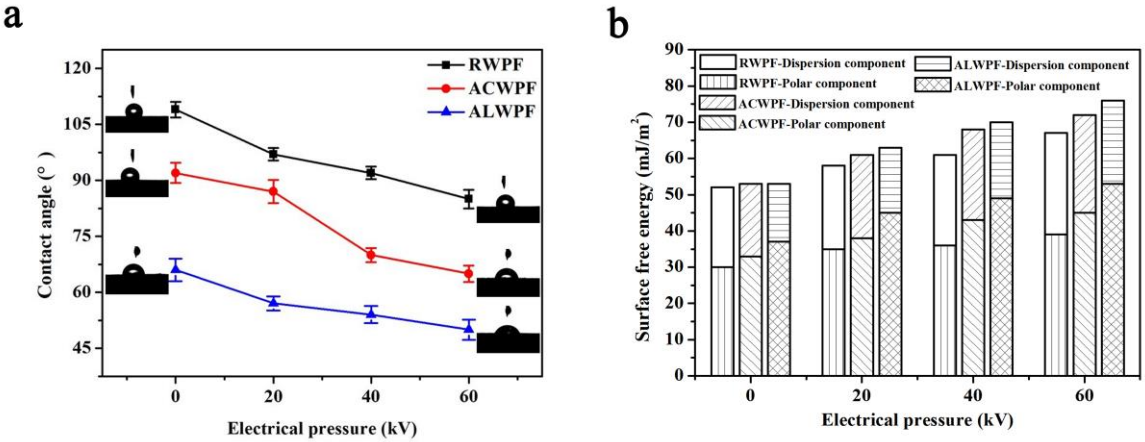

Figure 6 Distilled water contact angle (a) and surface energy (b) of WPF at different electrical pressures.

3.3 Performance evaluation of windmill palm fiber reinforced wood veneer composites

3.3.1 Micrographs of the Bonding Interphase

The interface of WPF reinforced plywood with different HVEF treatments was analyzed by SEM, and the results are shown in **Fig. 7**. From the result of **Fig. 7a**, it can be concluded that the distribution of adhesive at the untreated bonding interface is dispersed and disordered. After HVEF treatment (**Fig. 7b**), the penetration depth of adhesive on both sides of the

bonding interface decreased significantly, and the tracheid was filled with more PF adhesive at the interface. It can also be seen that the distribution of PF adhesive at the bonding interface was more continuous and regular. These results are in accordance with the fact that the polarization and oxidation degree of the surface of the material are improved by HVEF treatment [45]. Therefore, HVEF can limit the penetration of glue from tracheid cavity, pit and gap into the internal structure deeper from the interface, and improve the chemical cross-linking reaction between adhesive and wood at the interface.

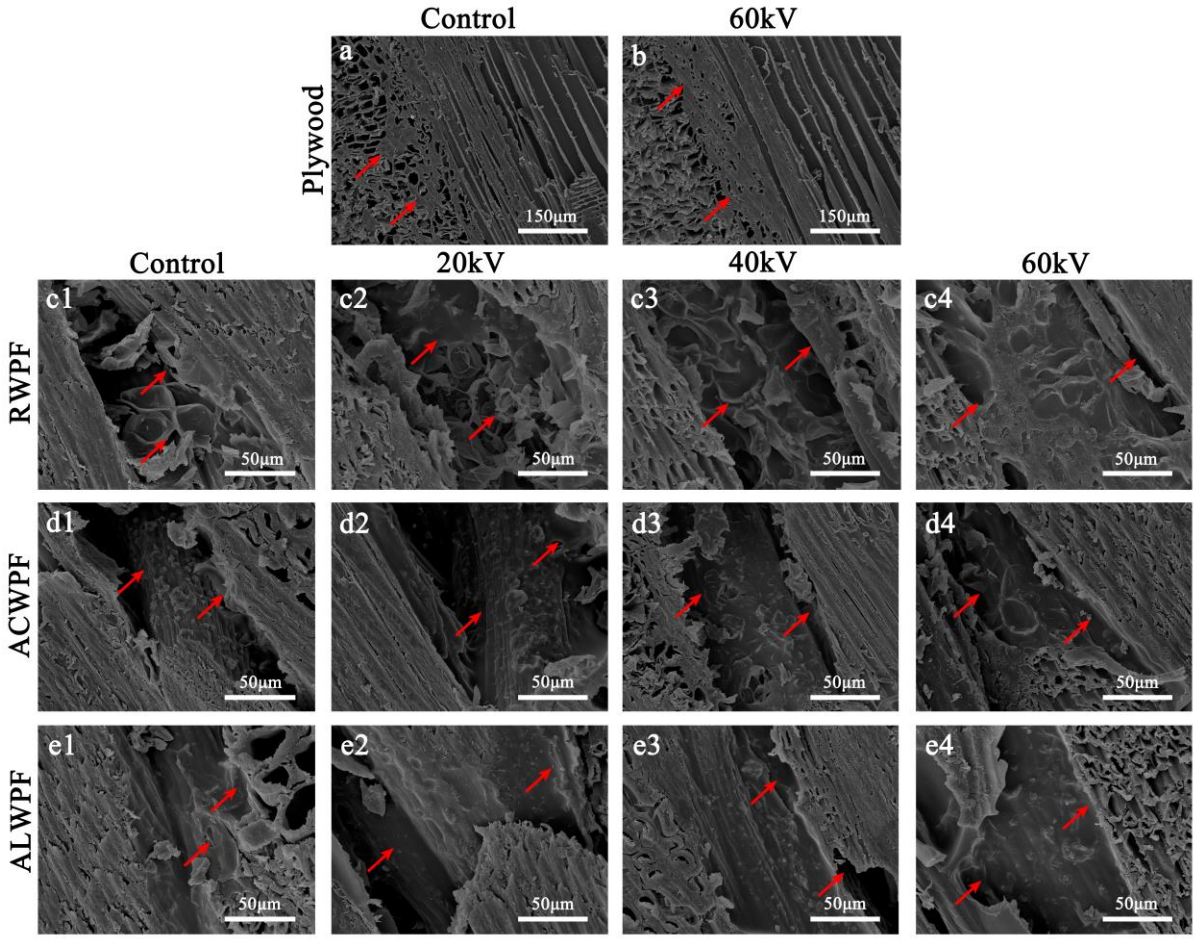

Figure 7 Micrographs obtained from the WPF reinforced wood veneer composites bonding interphase with different treatment parameters.

According to the micrographs of **Fig. 7c1**, **7d1** and **7e1**, it can be observed the surface of

489 untreated fibers (Fig. **7c1**) appeared to be free of adhesive indicating a poor fiber-matrix
490 adhesion. An increase of the interfacial adhesion was observed for ACWPF and ALWPF
491 probably because of the removal of the silica particles and scaly substances on the surface of
492 palm fiber previously described [48]. Compared with the HVEF treated bonding interface, PF
493 treated HVEF can cover the fiber and improve the interface adhesion, so as to enhance the
494 adhesion between fiber and matrix. After 20 kV HVEF treatment, the area of WPF covered by
495 PF increased (as shown in **Fig. 7c2**, **7d2** and **7e2**). This can be attributed to the HVEF
496 treatment, which can stimulate the oxygen-containing functional groups on the surface of
497 WPF in a short time, improve the hydrophilicity of WPF surface, and a large number of
498 excited electrons and broken chemical bonds (oxygen-containing groups) to collide with the
499 PF, thus increasing the cross-linking reaction of the PF [45, 49]. When the HVEF treatment
500 voltage increased from 20kV to 60kV, the PF coverage on the surface of WPF further
501 increased (as shown in **Fig. 7c4**, 7**d4** and 7**e4**). Therefore, HVEF can limit the penetration of
502 glue from tracheid cavity, pit and gap into the internal structure deeper from the interface, and
503 improve the chemical cross-linking reaction between adhesive and wood at the interface.
504 A comparison of the with three WPF reinforced Plywood under 60kV (**Fig. 7c4**, 7**d4** and
505 7**e4**) showed thatt the bonding interface of ALWPF-reinforced plywood is the best, the PF
506 distribution being continuous and uniform, and the fiber surface being completely covered
507 with PF. Under HVEF treatment, the surface wettability was higher, and more
508 oxygen-containing functional groups (consistent with the results of XPS analysis) were
509 excited to crosslink with the PF, which improved the interfacial properties.

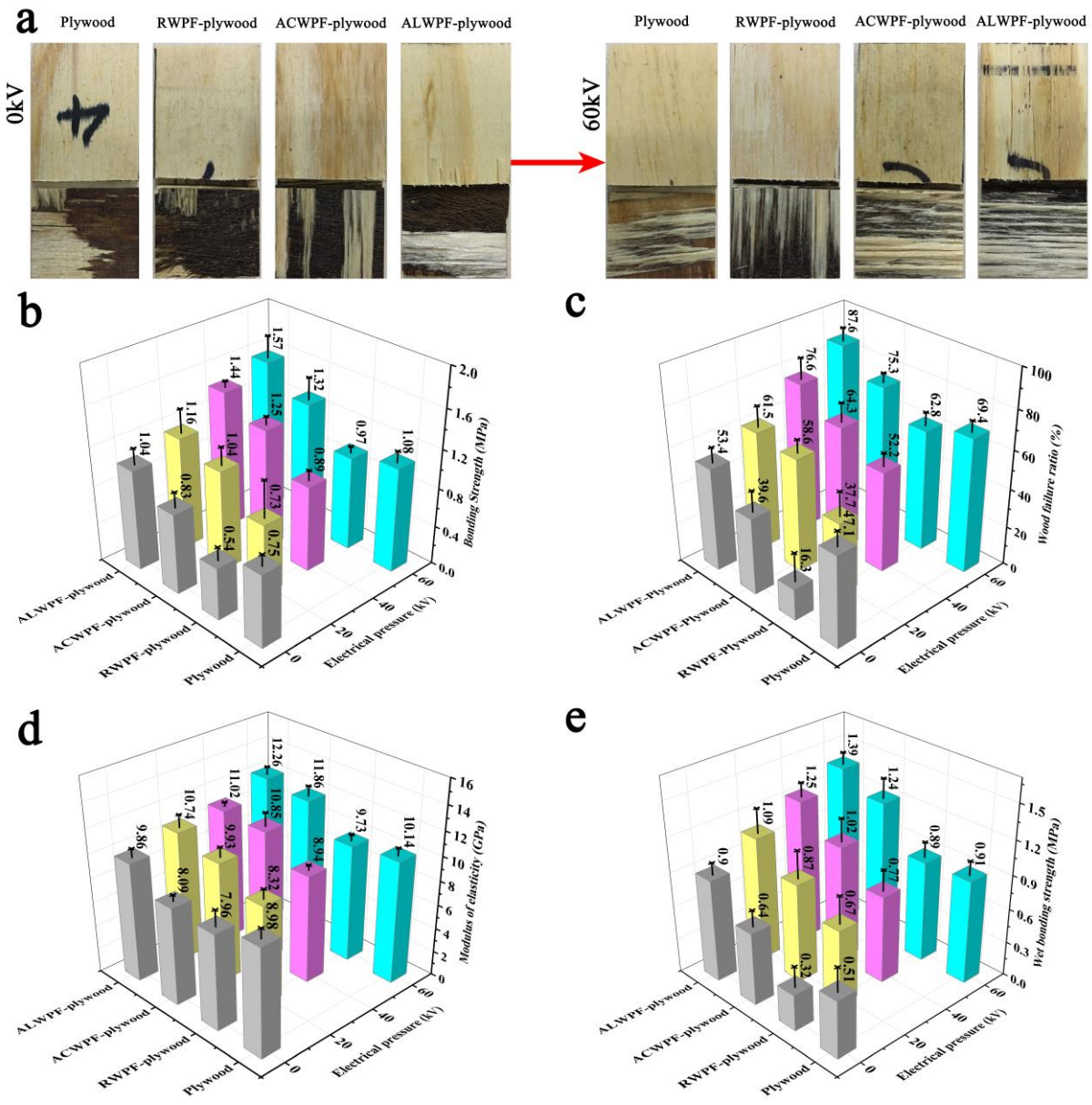

510

511 **Figure 8** Fracture surface analysis (a). The bonding strength (b), wood failure ratio (c), MOE

512 (d), and wet bonding strength (e) of WPF reinforced wood veneer composites with different

513 treatment parameters.

514

515 3.3.2 *Mechanical properties test*

516 The mechanical properties of WPF reinforced plywood were analyzed by bonding strength

517 (BS), wood failure ratio, modulus of elasticity (MOE) and wet bonding strength (WBS). As

shown in **Fig. 8b**, the mechanical properties increased in the order RWPF < ACWPF < ALWPF confirming the impact of the alkaline or acidic pretreatment on the properties of the composite. It can also be seen that HVEF treatment can further significantly improve the properties of the plywood. For ALWPF reinforced plywood, the BS was increased from 1.16 MPa to 1.44 MPa then to 1.57 MPa when HVEF voltage increased from 20 kV to 40 kV and to 60 kV. It can be found a synergistic effect between the alkaline or acidic pretreatment and the HVEF treatment, leading to an overall bonding strength of ALWPF and ACWPF reinforced plywood better than that of plywood. From **Fig. 8a** and **8c**, it can be observed that HVEF treatment can significantly improve the wood failure ratio.

Digital image correlation (DIC) technology, a non-contact high-precision displacement, deformation and motion measurement method, has the advantages of simple light path, little external influence and low requirements for vibration isolation conditions [50]. In this experiment, DIC technology was used to analyze the shear strain distribution of WPF reinforced plywood before and after HVEF (60kV) treatment (**Fig. 9b**). **Fig. 9a** shows the tensile shear strain measurement process. Under the action of tensile stress, the internal structure of plywood deformed to a certain extent. When the load reached the elastic limit value, subtle cracks appeared in the weak area of the sample and they gradually expanded, leading to tensile failure of the plywood.

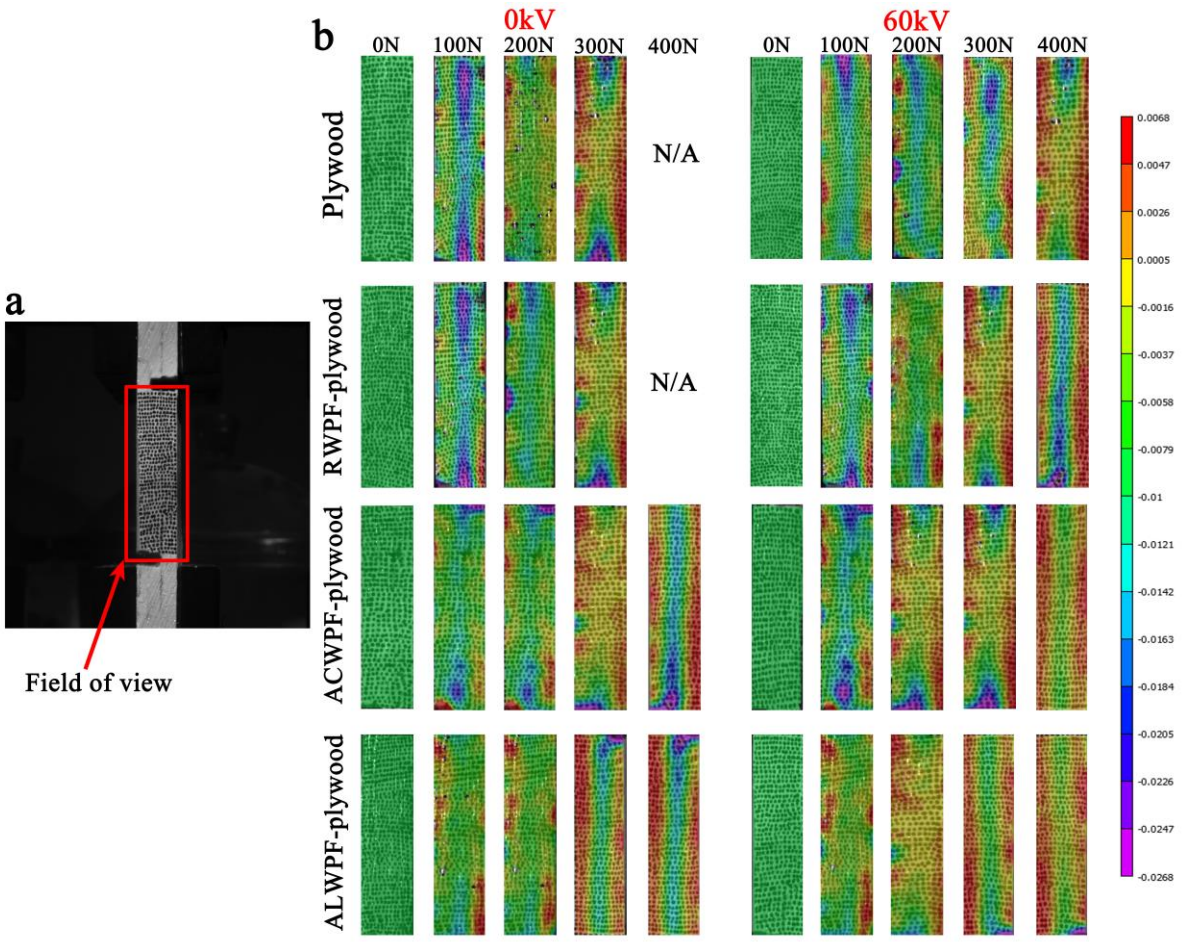

Figure 9 Tensile shear strain measurement (a), the tensile shear strain distribution (b) of WPF reinforced wood veneer composites with different treatment parameters

Deformation after HVEF treatment (60kV) occurs at a higher stress than that of untreated plywood. The reason is that the PF of untreated plywood penetrates into the veneer along the crack of the veneer, and it is easier to disperse the stress from the main glue layer to the wood matrix, resulting in the absence of PF in the main glue layer and the deterioration of mechanical properties. As a result, after HVEF treatment the uniform and continuous glue layer previously observed at the bonding interface significantly improved the mechanical properties. For the shear strain of WPF reinforced plywood, it can be seen that the strain distribution of the tensile interface on both sides of the plywood is relatively uniform under

549 the load of 100 N. For 200N, deformation is observed at both ends under the action of tensile
550 stress with an increase in the value of the deformation. When the load reached 300 N, the
551 strain concentration of RWPF and ACWPF reinforced plywood appears to be more important.
552 In contrast, the ALWPF and HVEF samples show a clear and regular deformation field, the
553 deformation zone gradually extending in the length direction and the deformation zone being
554 relatively concentrated. These results indicate that acid/alkali treated WPF can reduce the
555 tensile stress concentration in plywood. The HVEF treatment has a significant effect on the
556 strain distribution in the shear section, leading to an improvement in both the strain transfer in
557 the shear section and the mechanical properties of WPF-reinforced plywood.

558 The bending properties of WPF reinforced plywood were analyzed by three-point bending
559 test (**Fig. 8d**). It was found that the bending properties of WPF reinforced plywood were
560 positively affected by HVEF treatment of 60kV, and the MOE of ALWPF (60kV) reinforced
561 plywood was increased by 36.5%. **Fig. 8e** shows the BS of plywood after cooking in boiling
562 water for 4h and drying in oven-dried at 63 ℃ for 20h according to Chinese National
563 Standard (GB/T 9846-2015) [51]. A strong decrease in BS for untreated WBS and RWPF
564 plywoods of 32% and 41% respectively was observed while the decrease in BS was more
565 limited for the acid / alkali reinforced plywood and HVEF treated samples (25% and 15%
566 respectively). Therefore, HVEF can effectively inhibit the decrease of BS after cooking.

567

568 **Conclusion**

569 Alakli pretreatments of wind palm fibers have significantly improved their surface
570 properties by removing silica particles and scales. An improvement in their mechanical

properties was also observed. Modulus and tensile strength were increased by 167.07% and 26.52% respectively. HVEF can improve the polarization and oxidation degree of the WPF surface, and increase the reactive groups contents on the fiber surface (– OH and – CHO). Due to the synergistic effect of acid / alkali pretreatment and 60 kV HVEF treatment, the interfacial properties of reinforced plywood were effectively improved and the strain distribution of the composite was more uniform. Compared with unreinforced plywood, the BS and MOE were increased by 109.33% and 36.53% respectively. We hope that this process will allow a better use of wind palm fibers for the design of innovative wood composite materials.

Declaration of Competing Interest

The authors declare that they have no known competing financial interests or personal relationships that could have appeared to influence the work reported in this paper.

Acknowledgements

The authors gratefully acknowledge funding supports from the National Natural Science Foundation of China (32071700), the Natural Science Foundation of Jiangsu Province (CN) (No. BK20170926), a Project Funded by the National First-class Disciplines (PNFD), a Project Funded by the Priority Academic Program Development of Jiangsu Higher Education Institutions (PAPD), and the advanced analysis and testing center of Nanjing Forestry University. Zehui Ju also obtained the grand from the China Scholarship Council. LERMAB is supported by the French National Research Agency through the Laboratory of Excellence

ARBRE (ANR-12- LABXARBRE-01).

Reference

[1] W. Zhang, P. Yang, Y. Cao, et al., Evaluation of fiber surface modification via air plasma on the interfacial behavior of glass fiber reinforced laminated veneer lumber composites, Constr. Build. Mater. 233 (2020) 117315.

[2] B.C. Bal, Flexural properties, bonding performance and splitting strength of LVL reinforced with woven glass fiber, Constr. Build. Mater. 51 (2014) 9-14.

[3] H. Xu, T. Nakao, C. Tanaka, et al., Effects of fiber length and orientation on elasticity of fiber-reinforced plywood, J. Wood. Sci. 44(5) (1998) 343-353.

[4] O. Percin, M. Altunok, Some physical and mechanical properties of laminated veneer lumber reinforced with carbon fiber using heat-treated beech veneer, Eur. J. Wood. Wood. Prod. 75 (2) (2016) 193-201.

[5] M. Subhani, A. Globa, R. Al-Ameri, et al., Effect of grain orientation on the CFRPto-LVL bond, Composites Part B 129 (2017) 187-197.

[6] Z. Zhang, Q. Lei, R. He, et al., Review on antibacterial biocomposites of structural laminated veneer lumber, Saudi. J. Biol. Sci. 23(1) (2016) 142-147.

[7] B.C. Bal, The effect of span-to-depth ratio on the impact bending strength of poplar LVL, Constr. Build. Mater. 112 (2016) 355-359.

[8] F.Ahmad, N. Yuvaraj, P.K. Bajpai, Effect of reinforcement architecture on the macroscopic mechanical properties of fiberous polymer composites: A review, Polym. Composite. 41(6) (2020) 2518-2534.

615 [9] A.A. Gholampour, T. Ozbakkaloglu, A review of natural fiber composites: properties,
616 modification and processing techniques, characterization, applications, J. Mater. Sci. 55
617 (2019) 829-892.
618 [10] A.L. Duigou, A. Bourmaud, C. Gourier , C. Baley, Multi-scale shear properties of flax
619 fibre reinforced polyamide 11 biocomposites, Compos. Part A-Appl. S. 85 (2016)
620 123-129.
621 [11] A.M. O'Donnell, M.A. Dweib, R. P. Wool, Natural fiber composites with plant oil-based
622 resin, Compos. Sci. Technol. 64 (2004) 1135-1145.
623 [12] L. Yan, N. Chouw, Behavior and analytical modeling of natural flax fibre-reinforced
624 polymer tube confined plain concrete and coir fibre-reinforced concrete. J. Compos.
625 Mater. 47 (2012) 2133-2148.
626 [13] M.L. Loong, D. Cree, Enhancement of mechanical properties of bio-resin epoxy/flax
627 fiber composites using acetic anhydride, J. Polym. Environ. 26 (2018) 224-234.
628 [14] B.C. Bal, I. Bektas, F. Mengelog˘lu, et al., Some technological properties of poplar
629 plywood panels reinforced with glass fiber fabric, Constr. Build. Mater. 101 (1) (2015)
630 952-957.
631 [15] H. Luo, H. Zhang, L. Yue, et al., Effects of steam explosion on the characteristics of
632 windmill palm fiber and its application to fiberboard. Eur. J. Wood. Wood. Prod. 76(2)
633 (2018) 601-609.
634 [16] S. Zhai, D. Li, B.Pan, et al., Tensile strength of windmill palm (Trachycarpus fortunei)
635 fiber bundles and its structural implications, J. Mater. Sci. 47(2) (2012) 949-959.
636 [17] J. Li, X. Zhang, J. Zhu, et al., Structural, chemical, and multi-scale mechanical

637 characterization of waste windmill palm fiber (Trachycarpus fortunei), J. Wood. Sci.
638 66(1) (2020) 1087.
639 [18] S.K. Sundaram, S. Jayabal, Mechanical properties of potassium hydroxide-pretreated
640 Christmas palm fiber-reinforced polyester composites: characterization study, modeling
641 and optimization, J. Polym. Eng. 34(9) (2014) 839-849.
642 [19] Z. Ju, Q. He, H. Zhang, et al., Steam explosion of windmill palm fiber as the filler to
643 improve the acoustic property of rigid polyurethane foams, Polym. Composite. 41(7)
644 (2020) 2893-2906.
645 [20] P.B. Tomlinsin, The Structural Biology of Palms, Oxford University Press. USA.
646 (1990).
647 [21] C. Chen, Z. Wang, Y. Zhang, et al., Investigation of the hydrophobic and acoustic
648 properties of bio windmill palm materials, Sci. Rep-UK. 8 (1) (2018) 13419.
649 [22] A. Alawar, A.M. Hamed, K. Alkaabi, Characterization of treated date palm tree fiber as
650 composite reinforcement, Compos. Part. B-Eng. 40 (7) (2009) 601-606.
651 [23] N.Shanmugasundaram, I. Rajendran, T. Ramkumar, Characterization of untreated and
652 alkali treated new cellulosic fiber from an Areca palm leaf stalk as potential
653 reinforcement in polymer composites, Carbohyd. Polym. 195 (2018) 566-575.
654 [24] B.A. Kemp, I. Nikolayev, C.J. Sheppard, Coupled electrostatic and material surface
655 stresses yield anomalous particle interactions and deformation, J. Appl. Phys. 119 (14)
656 (2016) 1-7.
657 [25] O. Schnitzer, E. Yariv, The Taylor-Melcher leaky dielectric model as a macroscale
658 electrokinetic description, J. Fluid. Mech. 773 (2015) 1-33.

[26] A. Kilic, E. Shim, B. Pourdeyhimi, Measuring electrostatic properties of fibrous materials: A review and a modified surface potential decay technique, J. Electrostat. 74(4) (2015) 21-26.

[27] J. Dzubiella, R.J. Allen, J.-P. Hansen, Electric field-controlled water permeation coupled to ion transport through a nanopore, J. Chem. Phys. 120 (11) (2004) 5001.

[28] S. Erik, T.-A. Thomas, P. Thomas, S. Ullrich, Electrically induced structure formation and pattern transfer, Nature. 403 (6772) (2000) 874-877.

[29] T. Hattori, T. Tamura, On the effect of electricity upon the growth of wood-destroying fungi, J. Phytopathol. 9 (1939) 211-222.

[30] L.C. Segal, J. Creely, A.E.J. Martin, et al., An empirical method for estimating the degree of crystallinity of native cellulose using the X-Ray diffractometer, Text. Res. J. 29 (10) (1959) 786-94.

[31] A. Bill, B. John, NREL Laboratory Analytical Procedure, NREL/LAP-006 (1996) .

[32] American Society for Testing and Materials. ASTM C1557-14. Standard Test Method for Tensile Strength and Young's Modulus of Fibers, ASTM: Danvers, (2014).

[33] European Standard. EN-310-1993. Wood-based panels-Determination of modulus of elasticity in bending and of bending strength, CEN: (1993).

[34] China National Standard. GB / T 19536-2015. Plywood for container flooring, (2015).

[35] C. Chen, G. Chen, Z. Wang, et al., Optimization for alkali extraction of windmill palm fibril, J. Text. I. 109 (5) (2017) 1-7.

[36] C. Chen, G. Chen, X. Li, et al., The influence of chemical treatment on the mechanical properties of windmill palm fiber, Cellulose. 24(2) (2017) 1611-1620.

681 [37] E. Bodros, C. Baley, Study of the tensile properties of stinging nettle fibres (Urtica
682 dioica), Mat. Lett. 62 (2008) 2143-5.
683 [38] M.A. Norul Izani, M.T. Paridah, U.M.K. Anwar, et al., Effects of fiber treatment on
684 morphology, tensile and thermogravimetric analysis of oil palm empty fruit bunches
685 fibers, Compos. Part. B-Eng. 45 (1) (2013) 1251-1257.
686 [39] D. Shanmugam, M. Thiruchitrambalam, Static and dynamic mechanical properties of
687 alkali treated unidirectional continuous Palmyra Palm Leaf Stalk Fiber/jute fiber
688 reinforced hybrid polyester composites, Mater. Design. 50 (2013) 533-542.
689 [40] G.W. Beckermann, K.L. Pickering, N.J. Foreman, The processing, production and
690 improvement of hemp-fibre reinforced polypropylene composite materials, In: Proc of
691 2nd international conference on structure, processing and properties of materials. (2004)
692 257-265.
693 [41] Z. Ju, T. Zhan, H. Zhang, et al., Strong, durable, and aging-resistant bamboo composites
694 fabricated by silver in situ impregnation, ACS Sustainable Chem. Eng. 8 (2020)
695 16647−16658.
696 [42] Q. He, T. Zhan, Z. Ju, et al., Influence of high voltage electrostatic field (HVEF) on
697 bonding characteristics of Masson (Pinus massoniana Lamb.) veneer composites, Eur. J.
698 Wood Wood Prod. 77 (2019) 105-114.
699 [43] P. Nzokou, D.P. Kamdem, X-ray photoelectron spectroscopy study of red oak-(Quercus
700 rubra), black cherry-(Prunus serotina) and red pine-(Pinus resinosa) extracted wood
701 surfaces, Surf. Interface. Anal. 37 (2010) 689-694.
702 [44] Q. He, T. Zhan, H. Zhang, et al., Variation of surface and bonding properties among four

703 wood species induced by a high voltage electrostatic field (HVEF), Holzforschung.
704 73(10) (2019) 957-965.
705 [45] Z. Ju, T. Zhan, H. Zhang, et al., Preparation of functional bamboo by combining
706 nano-copper with hemicellulose and lignin under high voltage electric field (HVEF),
707 Carbohyd. Polym. 250 (2020) 116936.
708 [46] J. Ciscar, D. Pratelli, M. Abel, et al. Surface characterisation of pine wood by XPS, Surf.
709 Interface. Anal. 48 (7) (2016) 589-592.
710 [47] N. Monrolin, O. Praud, F. Plourabou, Electrohydrodynamic ionic wind, force field, and
711 ionic mobility in a positive dc wire-to-cylinders corona discharge in air, Phys. Rev.
712 Fluids. 3 (6) (2018) 1-10.
713 [48] N. Ramlee, M. Jawaid, S.A.K. Yamani, et al., Effect of surface treatment on mechanical,
714 physical and morphological properties of oil palm/bagasse fiber reinforced phenolic
715 hybrid composites for wall thermal insulation application, Constr. Build. Mater. 276
716 (2021) 122239.
717 [49] V. Cech, A. Marek, A. Knob, et al., Continuous surface modification of glass fibers in a
718 roll-to-roll plasma enhanced CVD reactor for glass fiber/polyester composites,
719 Composites Part A 121 (2019) 244-253.
720 [50] H.J. Kang, Z. Wang, Y.Y. Wang, et al., Development of mainly plant proteinderived
721 plywood bioadhesives via soy protein isolate fiber self-reinforcedsoybean meal
722 composites, Ind. Crop. Prod. 133 (2019) 10-17.
723 [51] Chinese National Standard GB/T 9846-2015, Plywood for general use.